Slow and Fast Singlet Energy Transfers in BODIPY-gallium(III)corrole Dyads Linked by Flexible Chains

Bertrand Brizet,[†,‡] Nicolas Desbois,[†] Antoine Bonnot,[‡] Adam Langlois,[‡] Adrien Dubois,[†] Jean-Michel Barbe,[†] Claude P. Gros,*[,†] Christine Goze,*[,†] Franck Denat,[†] and Pierre D. Harvey*[,‡]

[†]ICMUB (UMR 6302), Université de Bourgogne, Dijon, France
[‡]Département de Chimie, Université de Sherbrooke, Sherbrooke, Québec, Canada

Ⓢ *Supporting Information*

ABSTRACT: Red (no styryl), green (monostyryl), and blue (distyryl) BODIPY-gallium(III) (BODIPY = boron-dipyrromethene) corrole dyads have been prepared in high yields using click chemistry, and their photophysical properties are reported. An original and efficient control of the direction of the singlet energy transfers is reported, going either from BODIPY to the gallium-corrole units or from gallium-corroles to BODIPY, depending upon the nature of the substitution on BODIPY. In one case (green), both directions are possible. The mechanism for the energy transfers is interpreted by means of through-space Förster resonance energy transfer (FRET).
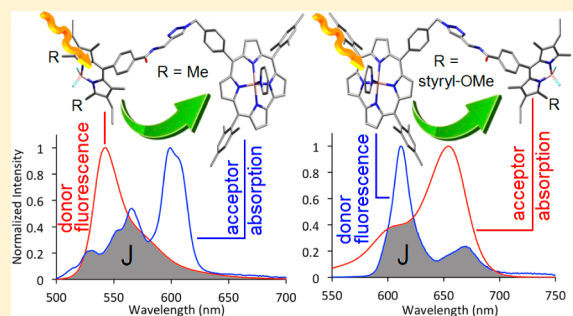
INTRODUCTION

Efforts have recently been devoted for the design of porphyrin−BODIPY (BODIPY = boron-dipyrromethene) dyads acting mainly as light-harvesting antennas for the photochemical conversion of solar energy.[1] In almost all reported examples, the role of the BODIPY unit was to essentially fill the blue-green region of the visible spectrum where porphyrins absorb weakly (i.e., between the Soret and Q-bands). Indeed, increasing the number of chromophore molecules can contribute to cover absorption in the entire visible spectrum resulting in, for example, a panchromatic light capture. In this respect, other recent developments on porphyrin−BODIPY dyad indeed focused on a novel broadband capturing and emitting system useful for solar energy harvesting.[2]

Concurrently, our group explored over a few years the chemistry of corrole macrocycles, akin to porphyrins but with one less meso carbon atom in their outer periphery.[3] Literature investigations show that the insertion of gallium(III) into the corrole macrocycle can efficiently enhance corrole fluorescence intensity.[4] This property is of prime importance for the potential use of corroles in medicinal applications[5] and photophysics[6] particularly as fluorescent probes. This feature becomes even more appealing if these corrole macrocycles are incorporated into polychromophoric arrays. The first corrole gallium(III) complex as well as its X-ray structure were reported by Gross et al.[7] The metalation of the corrole free base by GaCl₃ was shown to be convenient and preceded in almost quantitative yields.

Recently, we reported the synthesis and spectroscopic characterization of new zinc porphyrin−BODIPY dyads that exhibit efficient singlet energy transfers. In one case, energy transfer occurs from BODIPY to the porphyrin,[8] whereas, in the case of blue π-conjugated BODIPY−zinc porphyrin tweezers, the energy transfer occurs in the opposite direction, for example, from the photoexcited singlet zinc porphyrin to the π-conjugated BODIPY moiety of the composites as compared to energy transfer from the singlet excited state of conventional BODIPY to zinc porphyrins.[9]

We now report the synthesis and spectroscopic characterization of new covalently linked red (no styryl), green (styryl-monosubstituted), and blue (styryl-disubstituted)-BODIPY-gallium(III) corrole derivatives bridged by triazole linkers (Chart 1; see the real color of the solutions in Supporting Information, Figure S1). To the best of our knowledge, no previous example of a corrole macrocycle covalently linked to BODIPY has been reported. It is noteworthy that an original and efficient control of the direction of the singlet energy transfers is herein reported, for example, from BODIPY to the gallium-corrole units or from gallium-corroles to BODIPY, depending upon the nature of the BODIPY (blue, green, or red).
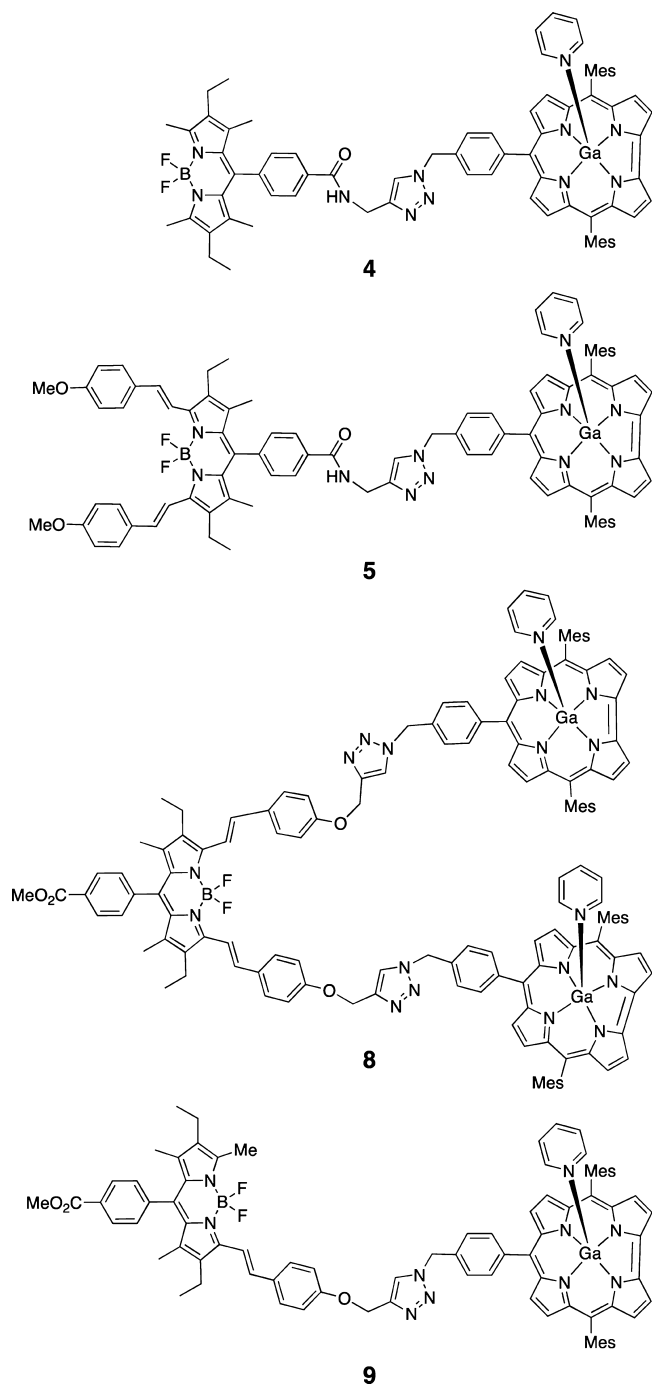
EXPERIMENTAL SECTION

Materials. Unless otherwise stated, all chemicals and solvents were of analytical reagent grade and were used as received. Absolute dichloromethane was obtained from Carlo Erba. Silica gel (Merck; 70−120 mm) was used for column chromatography. Analytical thin-layer chromatography (TLC) was performed with Merck 60 F₂₅₄ silica gel (precoated sheets, 0.2 mm thick). Reactions were monitored by thin-layer chromatography, ultraviolet−visible (UV−vis) spectroscopy,

Chart 1. Structure of the Different BODIPY−Corrole Dyads

rescence emission and excitation spectra were obtained on a Fluorolog SPEX 1680 0.22 m double monochromator spectrometer using quartz cuvettes (1 cm, 3 mL). All fluorescence spectra were corrected for apparatus response. Fluorescence lifetimes were measured on an apparatus that incorporated a nitrogen laser as the source and a high-resolution dye laser (full width at half-maximum (fwhm) = 1.4 ns). Fluorescence lifetimes were obtained from high-quality decays and deconvolution or distribution lifetime analysis. The uncertainties ranged from 20 to 40 ps on the basis of multiple measurements.

Quantum Yield Measurements. Measurements were performed in distilled 2-methyltetrahydrofuran (2-MeTHF), and spectrophotometric grade methanol (Aldrich) was used for references. Quartz cuvettes of 3 mL with path length of 1 cm equipped with a septum were used, and all solutions were Ar-degassed prior to measurements. Three different measurements (i.e., different solutions) were performed for each quantum yield. The sample concentrations were chosen to obtain an absorbance of about 0.05. The fluorescence quantum yield (Φ_F) measurements were performed with the slit width of 0.5−1.5 nm for both excitation and emission. Relative quantum efficiencies were obtained by comparing the areas under the corrected emission spectra of the sample relative to a known standard, and the following equation was used to calculate quantum yield: $\Phi_F(\text{sample}) = \Phi_F(\text{standard}) \ (I_{\text{sample}}/I_{\text{standard}}) \ (A_{\text{standard}}/A_{\text{sample}}) \ (\eta_{\text{sample}}^2/\eta_{\text{standard}}^2)$, where $\Phi_F(\text{standard})$ is the reported quantum yield of the standard, I is the integrated emission spectrum, A is the absorbance at the excitation wavelength, and η is the refractive index of the solvents used. Rhodamine 6G ($\Phi_F = 0.94$ in methanol),[10] cresyl violet ($\Phi_F = 0.54$ in methanol),[11] and rhodamine 101 ($\Phi_F = 1.00$ in methanol)[12] were used as standards.[13] In all Φ_F determinations, correction for the solvent refractive index (η) was applied (in 2-MeTHF, $\eta = 1.406$; in methanol, $\eta = 1.328$).[14]

DFT Calculations. All computer modeling was performed using the density functional theory (DFT) and Gaussian 09[15] at the Université de Sherbrooke with the Mammouth supercomputer supported by Le Réseau Québécois De Calculs Hautes Performances. The DFT geometry optimizations[16] were carried out using the B3LYP method. A 6-31g* basis set was used for C, H, N, and F atoms. VDZ (valence double ζ) with SBKJC effective core potential was used for B and Ga atoms.[17]

Synthesis of 10-(4-azidomethylphenyl)-5,15-dimesitylcorrole gallium(III)(pyridine) (1). 10-(4-Azidomethylphenyl)-5,15-dimesitylcorrole[3a] (50.0 mg, 0.075 mmol) was added to a 0.114 M solution of GaCl₃ in dry pyridine (6.6 mL, 0.75 mmol). The reaction mixture was stirred to reflux for 1 h and 30 min, shielded from light. The solvent was removed, and the crude product was purified by column chromatography over silica (pentane−dichloromethane−pyridine, 100:30:0.5). The title compound **1** was isolated as a purple microcrystalline solid in 69% yield (42.0 mg, 0.052 mmol). ^{1}H NMR (300 MHz, CDCl₃) δ (ppm): 1.88 (s, 12H, CH₃), 2.61 (s, 6H, CH₃), 3.58 (m, 2H, H_Py), 4.66 (s, 2H, CH₂), 5.97 (m, 2H, H_Py), 6.76 (t, 1H, J = 7.8 Hz, H_Py), 7.26 (s, 4H, H_Mes), 7.63 (d, 2H, J = 8.1 Hz, H_Ph), 8.16 (d, 2H, J = 8.1 Hz, H_Ph), 8.55 (m, 4H, H_β), 8.62 (d, 2H, J = 4.5 Hz, H_β), 9.01 (d, 2H, J = 3.9 Hz, H_β). UV−vis (2-MeTHF): λ_{max} (nm) ($\varepsilon \times 10^{-3}$ L mol⁻¹ cm⁻¹) = 418 (206), 527 (7), 566 (13), 599 (26). MS (MALDI-TOF) m/z = 731.03 [M-pyridine]⁺, 731.23 calcd for C₄₄H₃₆GaN₇. HR-MS (ESI) m/z = 731.2263 [M-pyridine]⁺, 731.2283 calcd for C₄₄H₃₆GaN₇.

Compound 2. N-Hydroxybenzotriazole (959 mg, 7.10 mmol), diisopropylamine (995 μL, 7.10 mmol), 1-(3-dimethylaminopropyl)-3-ethylcarbodiimide hydrochloride (1.35 g, 7.10 mmol), and propargyl-amine (227 μL, 3.50 mmol) were successively added to a solution of BODIPY acid[18] (1.53 g, 3.50 mmol) in 100 mL of dimethylformamide (DMF), and the solution was stirred at RT. After total consumption of starting material (2 h) monitored by TLC, the solvent was evaporated. The resulting solid was washed with water (3 × 100 mL) and extracted with dichloromethane. The organic layer was dried over magnesium sulfate, and the solvent was evaporated to give a red oil. The crude product was purified by column chromatography on silica gel (dichloromethane/heptane 60:40) followed by a recrystallization in a mixture of dichloromethane and hexane to give a reddish solid in 72%

and matrix-assisted laser desorption ionization time-of-flight mass spectrometry (MALDI-TOF MS).

Instrumentation. The ^{1}H, ^{11}B, and ^{13}C NMR spectra were recorded at room temperature (RT) on a Bruker Avance II 300 (300 MHz) or on a Bruker Avance DRX 600 (600 MHz) spectrometer at the Welience, Pôle Chimie Moléculaire de l'Université de Bourgogne (WPCM). Chemical shifts (^{1}H NMR spectra) are expressed in ppm relative to chloroform (7.26 ppm) or pyridine (7.22, 7.58, 8.74). UV−vis spectra were recorded on a Varian Cary 300 Bio spectrophotometer. Mass spectra and accurate mass measurements (high-resolution (HRMS)) were obtained on a Bruker Daltonics Ultraflex II spectrometer in the MALDI-TOF reflectron mode using dithranol as a matrix or on a linear trap quadrupole (LTQ) Orbitrap XL (THERMO) instrument in electrospray ionization (ESI) mode. Both measurements were registered at WPCM. The steady-state fluo-

yield (1.15 g, 2.49 mmol). ^{1}H NMR (300 MHz, CDCl$_3$) δ (ppm): 0.96 (t, J = 7.5 Hz, 6H), 1.22 (s, 6H), 2.29 (q, J = 7.5 Hz, 4H), 2.30 (t, J = 2.5 Hz, 1H), 2.51 (s, 6H), 3.78 (dd, J = 2.5 Hz, J = 5.2 Hz, 2H), 6.27 (t, J = 5.2 Hz, 1H), 7.38 (d, J = 8.4 Hz, 2H), 7.91 (d, J = 8.4 Hz, 2H). ^{13}C NMR (75 MHz, CDCl$_3$) δ (ppm): 11.9, 12.5, 14.6, 17.1, 30.9, 72.1, 79.3, 127.8, 128.9, 130.4, 133.1, 134.0, 138.1, 138.5, 139.7, 154.3, 166.2. ^{11}B NMR (192.5 MHz, CDCl$_3$) δ (ppm): 0.78 (t, J = 33.4 Hz). UV–vis (2-MeTHF) λ_{max} (nm) ($\varepsilon \times 10^{-3}$ L mol^{-1} cm^{-1}): 238 (39), 494 (27), 525 (90). MS (ESI) m/z = 460.39 [M + H]$^+$, 484.34 [M + Na]$^+$. HRMS (ESI) 484.235 59 calcd for C$_{27}$H$_{30}$BF$_2$N$_3$ONa 484.234 70.

Compound 3. Compound **2** (100 mg, 0.22 mmol) and *p*-anisaldehyde (106 μL, 0.870 mmol) were dissolved in a mixture of dry toluene (40 mL), *p*-toluenesulfonic acid (PTSA, 6.0 mg, 0.035 mmol), and piperidine (752 μL, 7.60 mmol). The mixture was refluxed during 2 h in a Dean−Stark apparatus, and the solvent was removed in situ. Dry toluene (40 mL) and 750 μL of piperidine were added, and the mixture was refluxed for another 2 h. After total consumption of the starting material (monitored by UV−vis), the solvent was evaporated. The resulting solid was washed with water (3 × 100 mL) and extracted with dichloromethane. The organic layer was dried over magnesium sulfate, and the solvent was evaporated to give a blue solid. The crude product was purified by column chromatography on silica gel (heptane/CH$_2$Cl$_2$ 80:20), followed by a recrystallization in a mixture of dichloromethane and hexane to give a blue solid in 36% yield (55.0 mg, 78.8 μmol). ^{1}H NMR (300 MHz, CDCl$_3$) δ (ppm): 1.14 (t, J = 7.5 Hz, 6H), 1.28 (s, 6H), 2.32 (t, J = 2.5 Hz, 1H), 2.58 (q, J = 7.5 Hz, 4H), 3.84 (s, 6H), 4.30 (dd, J = 2.5 Hz, J = 5.2 Hz, 2H), 6.36 (t, J = 5.2 Hz, 1H), 6.93 (d, J = 8.7 Hz, 4H), 7.20 (d, J = 16.7 Hz, 2H), 7.43, (d, J = 8.3 Hz, 2H), 7.56 (d, J = 8.7 Hz, 4H), 7.65 (d, J = 16.7 Hz, 2H), 7.93 (d, J = 8.3 Hz, 2H). ^{13}C NMR (75 MHz, CDCl$_3$) δ (ppm): 11.8, 14.1, 18.4, 55.4, 72.2, 79.3, 114.3, 127.8, 128.9, 129.4, 130.3, 132.5, 133.9, 134.1, 135.8, 136.1, 138.3, 140.1, 150.9, 160.3, 166.3. ^{11}B NMR (192.5 MHz, CDCl3) δ (ppm): 1.23 (t, J = 34.2 Hz). UV−vis (2-MeTHF): λ_{max} (nm) ($\varepsilon \times 10^{-3}$ L mol^{-1} cm^{-1}): 250 (21), 334 (31), 368 (68), 608 (37), 654 (93). MS (ESI): m/z = 720.35 [M + Na]$^+$. HRMS (ESI) 720.320 39 calcd for C$_{43}$H$_{42}$BF$_2$N$_3$O$_2$Na 720.318 69.

Compound 6. BODIPY ester[18] (200 mg, 0.46 mmol) and 4-(prop-2-yn-1-yloxy)benzaldehyde (73.0 mg, 0.460 mmol) were dissolved in a mixture of dry toluene (20 mL), *p*-toluenesulfonic acid (PTSA, 50.0 mg, 0.290 mmol), and piperidine (989 μL, 10.0 mmol). The mixture was refluxed during 2 h in a Dean−Stark apparatus. The solvent was removed in situ, and 10 mL of dry toluene and 73 mg of 4-(prop-2-yn-1-yloxy)benzaldehyde were added. The mixture was refluxed for another 1 h, and solvent was removed. This step was repeated five times. After total consumption of starting material (monitored by UV−visible), the solvent was evaporated. The resulting solid was washed with water (3 × 50 mL) and extracted with dichloromethane. The organic layer was dried over magnesium sulfate, and the solvent was evaporated to give a blue solid. The crude product was purified by column chromatography on silica gel (dichloromethane/heptane 50:50), followed by a recrystallization in a mixture of dichloromethane and hexane to give **6** (133 mg, 184 μmol) in 40% yield as blue solid. ^{1}H NMR (300 MHz, CDCl$_3$) δ (ppm): 1.13 (t, J = 7.6 Hz, 6H), 1.28 (s, 6H), 2.53 (t, J = 2.4 Hz, 2H), 2,58 (q, J = 7.6 Hz, 4H), 3.97 (s, 3H), 4.73 (d, J = 2.4 Hz, 4H), 7.01 (d, J = 8.8 Hz, 4H), 7.20 (d, J = 16.6 Hz, 2H), 7.42 (d, J = 8.2 Hz, 2H), 7.56 (d, J = 8.8 Hz, 4H), 7.66 (d, J = 16.6 Hz, 2H), 8.20 (d, J = 8.2 Hz, 2H). ^{13}C NMR (75 MHz, CDCl$_3$) δ (ppm): 10.7, 13.0, 17.4, 51.4, 54.9, 74.7, 77.3, 114.2, 117.5, 127.8, 128.1, 129.3, 129.6, 130.1, 131.5, 133.0, 134.6, 137.4, 140.8, 149.8, 151.2, 157.1, 165.6. UV−vis (2-MeTHF): λ_{max} (nm) ($\varepsilon \times 10^{-3}$ L mol^{-1} cm^{-1}) = 255 (21), 332 (31), 366 (63), 428 (11), 604 (36), 654 (85). ^{11}B NMR (192.5 MHz, CDCl$_3$) δ (ppm): 1.20 (t, J = 34.6 Hz). MS (ESI): m/z = 745.30 [M + Na]$^+$. HRMS (ESI) 745.303 08 calcd for C$_{45}$H$_{41}$BF$_2$N$_2$O$_4$Na 745.302 73.

Compound 7. BODIPY ester[18] (1.10 g, 2.51 mmol) and 4-(prop-2-yn-1-yloxy)benzaldehyde (442 mg, 2.76 mmol) were dissolved in a mixture of dry toluene (50 mL), *p*-toluenesulfonic acid (PTSA, 53.0 mg, 0.308 mmol), and piperidine (3.3 mL, 33 mmol). The mixture was

refluxed during 2 h in a Dean−Stark apparatus, and the solvent was removed in situ. Dry toluene (50 mL) and piperidine (3 mL) were added, and the mixture was refluxed for another 2 h. After consumption of approximately a third of the starting material (monitored by UV−vis), the solvent was evaporated. The resulting solid was washed with water (3 × 100 mL) and extracted with dichloromethane. The organic layer was dried over magnesium sulfate, and the solvent was evaporated to give a blue solid. The crude product was purified by column chromatography on silica gel (dichloromethane/heptane 40:60), followed by a recrystallization in a mixture of dichloromethane and hexane to give **7** (73.0 mg, 125 μmol) in 5% yield. Compound **6** was also obtained as subproduct in 3% yield. ^{1}H NMR (300 MHz, CDCl$_3$) δ (ppm): 0.97 (t, J = 7.5 Hz, 3H), 1.12 (t, J = 7.5 Hz, 3H), 1.25 (s, 3H), 1.27 (s, 3H), 2.29 (q, J = 7.5 Hz, 2H), 2.52 (t, J = 2.4 Hz, 1H), 2.56 (s, 3H), 2.56 (q, J = 7.5 Hz, 2H), 3.97 (s, 3H), 4.71 (d, J = 2.4 Hz, 2H), 6.97 (d, J = 8.8 Hz, 2H), 7.16 (d, J = 16.8 Hz, 1H), 7.41 (d, J = 8.3 Hz, 2H), 7.54 (d, J = 8.8 Hz, 2H), 7.60 (d, J = 16.8 Hz, 1H), 8.16 (d, J = 8.3 Hz, 2H). ^{13}C NMR (75 MHz, CDCl$_3$) δ (ppm): 11.8, 12.1, 13.0, 14.3, 14.7, 17.3, 17.5, 18.5, 52.6, 56.1, 75.9, 78.6, 115.4, 118.6, 128.8, 129.1, 130.5, 130.9, 131.3, 131.6, 133.4, 134.0, 135.1, 138.0, 141.1, 150.0, 155.8, 158.2, 166.8. ^{11}B NMR (192.5 MHz, CDCl$_3$) δ (ppm): 0.98 (t, J = 33.8 Hz). UV−vis (2-MeTHF): λ_{max} (nm) ($\varepsilon \times 10^{-3}$ L mol^{-1} cm^{-1}) = 238 (19), 319 (17), 339 (29), 389 (8), 448 (27), 587 (81). MS (ESI): m/z = 603.4 [M + Na]$^+$. HRMS (ESI) 603.262 33 calcd for C$_{35}$H$_{35}$BF$_2$N$_2$O$_3$Na 603.260 71.

General Procedure for the Huisgen Reaction. 10-(4-Azidomethylphenyl)-5,15-dimesityl-corrole gallium(III)(pyridine) (30.0 mg, 37.0 μmol or 60.0 mg, 74.0 μmol for preparation of compound **8**) and BODIPY alkyne (37.0 μmol) were solubilized in 5 mL of THF. CuI (10.5 mg, 55.1 μmol or 21.0 mg, 110 μmol for preparation of compound **8**) and N,N-diisopropylethylamine (DIPEA) (14.0 μL, 148 μmol) were added. The mixture was stirred under N$_2$ at RT for 3 h. The crude mixture was evaporated to dryness. Then 20 mL of water was added. The compound was extracted with dichloromethane (3 × 20 mL). The collected organic solution was dried over MgSO$_4$, and the solvent was removed under reduced pressure. The product was recrystallized from CH$_2$Cl$_2$−hexane.

Compound 4. The title compound was isolated as a purple microcrystalline solid in 96% yield (45.0 mg, 35.4 μmol). ^{1}H NMR (300 MHz, pyridine-d_5) δ (ppm): 0.84 (m, 6H, CH$_3$), 1.20 (s, 6H, CH$_3$), 2.13 (m, 16H, CH$_2$, CH$_3$), 2.62 (s, 6H, CH$_3$), 2.70 (s, 6H, CH$_3$), 5.25 (d, 2H, J = 5.1 Hz, CH$_2$N), 6.05 (s, 2H, CH$_2$), 7.38 (m, 6H, H$_{mes}$, H$_{Ph}$), 7.49 (s, 1H, H$_{triazole}$), 7.76 (d, 2H, J = 7.8 Hz, H$_{Ph}$), 8.20 (d, 2H, J = 8.1 Hz, H$_{Ph}$), 8.46 (d, 2H, J = 8.1 Hz, H$_{Ph}$), 8.79 (m, 4H, H$_\beta$), 8.88 (d, 2H, J = 4.5 Hz, H$_\beta$), 9.25 (d, 2H, J = 3.9 Hz, H$_\beta$), 10.07 (m, 1H, NH). UV−vis (2-MeTHF): λ_{max} (nm) ($\varepsilon \times 10^{-3}$ L mol^{-1} cm^{-1}) = 419 (150), 525 (80), 567 (13), 600 (21). MS (MALDI-TOF) m/z = 1173.46 [M-pyridine-F]$^+$, 1173.47 calcd for C$_{71}$H$_{66}$BFGaN$_{10}$O. HR-MS (ESI) m/z = 1192.4762 [M-pyridine]$^+$, 1192.4744 calcd for C$_{71}$H$_{66}$BF$_2$GaN$_{10}$O.

Compound 5. The title compound was isolated as a purple microcrystalline solid in 97% yield (54.0 mg, 35.8 μmol). ^{1}H NMR (300 MHz, pyridine-d_5) δ (ppm): 1.04 (t, 6H, J = 7.2 Hz, CH$_3$), 1.24 (s, 6H, CH$_3$), 2.11 (s, 12H, CH$_3$), 2.56 (m, 10H, CH$_2$, CH$_3$), 3.65 (s, 6H, OCH$_3$), 5.25 (d, 2H, J = 5.1 Hz, CH$_2$N), 6.04 (s, 2H, CH$_2$), 6.91 (d, 2H, J = 8.7 Hz, H$_{Ph}$), 7.37 (m, 6H, H$_{mes}$, H$_{Ph}$), 7.50 (m, 3H, H$_{alkene}$, H$_{triazole}$), 7.71 (m, 6H, H$_{Ph}$), 8.19 (d, 2H, J = 8.1 Hz, H$_{Ph}$), 8.29 (d, 2H, J = 16.5 Hz, H$_{alkene}$), 8.47 (d, 2H, J = 8.1 Hz, H$_{Ph}$), 8.76 (m, 4H, H$_\beta$), 8.86 (d, 2H, J = 4.5 Hz, H$_\beta$), 9.23 (d, 2H, J = 3.9 Hz, H$_\beta$), 10.08 (m, 1H, NH). UV−vis (2-MeTHF): λ_{max} (nm) ($\varepsilon \times 10^{-3}$ L mol^{-1} cm^{-1}) = 368 (83), 419 (164), 605 (58), 654 (96). MS (MALDI-TOF) m/z = 1428.46 [M-pyridine]$^{·+}$, 1428.56 calcd for C$_{87}$H$_{78}$BF$_2$GaN$_{10}$O$_3$. HR-MS (ESI) m/z = 1428.5610 [M-pyridine]$^+$, 1428.5583 calcd for C$_{87}$H$_{78}$BF$_2$GaN$_{10}$O$_3$.

Compound 8. The title compound was isolated as a purple microcrystalline solid in 97% yield (84 mg, 35.8 μmol). ^{1}H NMR (300 MHz, pyridine-d_5) δ (ppm): 1.09 (m, 6H, CH$_3$), 1.29 (2s, 6H, CH$_3$), 2.13 (s, 24H, CH$_3$), 2.61 (m, 16H, CH$_2$, CH$_3$), 3.94 (s, 3H, OCH$_3$), 5.48 (s, 4H, CH$_2$), 6.07 (s, 4H, CH$_2$), 7.29 (m, 4H, H$_{Ph}$), 7.37 (m, 8H,

H$_{mes}$), 7.50 (m, 6H, H$_{triazole}$, H$_{alkene}$, H$_{Ph}$), 7.76 (m, 6H, H$_{Ph}$, H$_{Ph}$), 8.34 (m, 10H, H$_{Ph}$, H$_{alkene}$), 8.79 (m, 8H, H$_\beta$), 8.88 (d, 4H, J = 4.5 Hz, H$_\beta$), 9.24 (d, 4H, J = 3.9 Hz, H$_\beta$). UV–vis (2-MeTHF): λ_{max} (nm) ($\varepsilon \times$ 10^{-3} L mol^{-1} cm^{-1}) = 372 (63), 419 (244), 568 (32), 602 (60), 658 (63). MS (MALDI-TOF) m/z = 2165.76 [M-pyridine-F]$^+$, 2165.77 calcd for C$_{133}$H$_{113}$BFGa$_2$N$_{16}$O$_4$. HR-MS (ESI) m/z = 1092.8895 [M-2-pyridine]$^{2+}$, 1092.8832 calcd for C$_{133}$H$_{113}$BF$_2$Ga$_2$N$_{16}$O$_4$.

Compound 9. The title compound was isolated as a purple microcrystalline solid in 96% yield (49.5 mg, 35.6 μmol). ^{1}H NMR (300 MHz, pyridine-d_5) δ (ppm): 0.89 (t, 3H, J = 7.2 Hz, CH$_3$), 1.08 (t, 3H, J = 7.2 Hz, CH$_3$), 1.32 (2s, 6H, CH$_3$), 2.14 (m, 14H, CH$_2$, CH$_3$), 2.63 (m, 8H, CH$_2$, CH$_3$), 2.77 (s, 3H, CH$_3$), 3.93 (s, 3H, OCH$_3$), 5.52 (s, 2H, CH$_2$), 6.12 (s, 2H, CH$_2$), 7.35 (d, 2H, J = 8.4 Hz, H$_{Ph}$), 7.38 (m, 4H, H$_{mes}$), 7.50 (m, 4H, H$_{Ph}$, H$_{alkene}$, H$_{triazole}$), 7.76 (d, 2H, J = 8.4 Hz, H$_{Ph}$), 7.81 (d, 2H, J = 8.1 Hz, H$_{Ph}$), 8.33 (m, 5H, H$_{alkene}$, H$_{Ph}$), 8.80 (m, 4H, H$_\beta$), 8.89 (d, 2H, J = 4.5 Hz, H$_\beta$), 9.26 (d, 2H, J = 3.9 Hz, H$_\beta$). UV–vis (2-MeTHF): λ_{max} (nm) ($\varepsilon \times 10^{-3}$ L mol^{-1} cm^{-1}) = 340 (34), 418 (145), 591 (84). MS (MALDI-TOF) m/z = 1292.51 [M-pyridine-F]$^+$, 1292.50 calcd for C$_{79}$H$_{71}$BFGaN$_9$O$_3$. HR-MS (ESI) m/z = 1311.5018 [M-pyridine]$^+$, 1311.5004 calcd for C$_{79}$H$_{71}$BF$_2$GaN$_9$O$_3$.

■ RESULTS AND DISCUSSION

Synthesis. The azide-containing free base corrole (see starting product in Scheme 1) was prepared using the common

Scheme 1. Synthesis of Gallium-Corrole 1
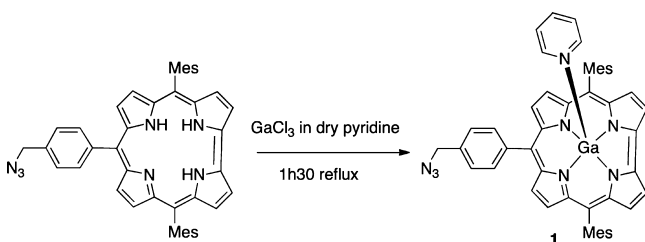
"2 + 1" method.[19] The preparation involves the condensation of an azidobenzyl aldehyde (1 equiv) with a mesityldipyrromethane (2 equiv) in the presence of a catalytic amount of trifluoroacetic acid (TFA, 0.08 equiv) using dichloromethane as solvent. Sterically hindered mesityldipyrromethane was used to avoid any acidolysis that could occur during the cyclization reaction.

Gallium(III) was inserted in the corrole cavity according to a literature procedure.[7,19] The inorganic salts were separated from the desired product by column chromatography on silica gel, affording the (pyridine)gallium(III) corrole **1** in 69% yield (Scheme 1). The formation of the gallium-corrole **1** was monitored by MALDI-TOF MS using the molecular peak at m/z = 731.2263 (731.2283 calcd for C$_{44}$H$_{36}$GaN$_7$), which shows a characteristic isotopic pattern corresponding to [M-pyridine]$^{·+}$. The coordination of one pyridine molecule to the gallium metal center was confirmed by ^{1}H NMR spectroscopy.

Ethynyl-functionalized BODIPY **2** was easily obtained by peptidic coupling between propargylamine and a BODIPY bearing a carboxylic group (generated from the methyl ester) in meso position as previously described in the literature.[20] The coupling reagent we used (Scheme 1) was based on a carbodiimide (e.g., 1-ethyl-3-(3-dimethylaminopropyl)-carbodiimide, EDCI·HCl) in the presence of 1-hydroxy-1H-benzotriazole (HOBt) and *N,N*-diisopropylethylamine (DIPEA). The ethylenic proton exhibits a triplet (δ = 2.30, ^4J_A = 2.5 Hz) in CDCl$_3$ ^{1}H NMR spectroscopy. The distyryl BODIPY **3** was synthetized using a reported method, which

consists in a Knoevenagel condensation between compound **2** and 4 equiv of *p*-anisaldehyde with *p*-toluenesulfonic acid (PTSA) and piperidine, in a Dean–Stark apparatus, using dry toluene as the solvent (Scheme 2).[9]

Similarly, the di- and monostyryl precursors **6** and **7** were respectively obtained using the same reaction, starting from carbomethoxy-*meso*-substituted BODIPY derivative and 4-(prop-2-yn-1-yloxy)benzaldehyde (Scheme 2). The reaction was monitored by UV–vis spectroscopy to obtain the maximal quantity of monocondensation product **7**. Difficulties in purification and formation of dicondensation subproduct **6** explain the low yield of reaction for **7** (5%). Nevertheless compound **6** can be obtained in good yield (40%) by using a larger quantity of 4-(prop-2-yn-1-yloxy)benzaldehyde, as described in the Experimental Section.

The Huisgen copper-catalyzed azide–alkyne cycloaddition, known as "click reaction,"[21] was used to efficiently link the BODIPY and the gallium-corrole subunits. Indeed, many reports have already mentioned the usefulness of the click chemistry for the elaboration of sophisticated structures involving mainly porphyrin as the backbone.[9,22] We applied a recent methodology described for the preparation of tripod porphyrins.[22] The reaction, catalyzed by CuI/di(isopropyl)-ethylamine (DIPEA), proceeds quantitatively in THF at RT for 3 h (Schemes 3 and 4). All BODIPY−Ga(III)-corroles were fully characterized by ^{1}H NMR spectroscopy in pyridine-d_5. HR-MS measurements were performed using an ESI-Orbitrap instrument to further confirm the successful formation of compounds **4**, **5**, **8**, and **9**. For example for compound **8**, the molecular peak is observed at m/z = 2165.76 [M-pyridine-F]$^+$ in the MALDI-TOF spectra, (2165.77 calcd for C$_{133}$H$_{113}$B-FGa$_2$N$_{16}$O$_4$), whereas by ESI HR-MS, the molecular peak appears at m/z = 1092.8895 [M-2-pyridine]$^{2+}$ (1092.8832 calcd for C$_{133}$H$_{113}$BF$_2$Ga$_2$N$_{16}$O$_4$).

Computer Modeling. To address whether the possible conformations due to the flexibility of the chain are energetically accessible, DFT geometry optimizations were performed for compounds **4** and **9**. The results from these computations are presented in Figure 1. Only representative examples are necessary to illustrate that many conformations of various energies coexist. The most stable conformations for **4** (and **5** due to their strong structural similarity) are the unfolded conformations C−E, differing by only the relative orientation of the C$_6$H$_4$CH$_2$ group in the chain. Concurrently, the unfolded and semifolded conformations D−F are noted to be the most stable ones for compound **9**, but the semifolded conformers B and C are only 1 kJ mol^{-1} destabilized with respect to the most stable ones. The folded conformer A is either too high in energy (**4**) or unstable (**9**). The conclusion is that many unfolded and semifolded conformers coexist in solution, but the folded conformer A is simply not accessible for **4** and **9**.

Electronic Absorption Spectra. Table 1 summarizes the UV−vis data for all compounds in 2-MeTHF. Compound **1** exhibits one Soret band at 418 nm and three Q bands at 527, 566, and 599 nm of the corrole chromophore. Compounds **2**, **3**, **6**, and **7** exhibit bands characteristic of the BODIPY chromophore; the S$_0$−S$_1$ band at 525, 654, 587, and 658 nm is assigned to spin-allowed π−π* transitions. Dyads **4**, **5**, **8**, and **9** display the expected corrole Soret band and Q bands in addition to the BODIPY π−π* transitions. The absorption spectra of the dyads are simply the sum of the individual chromophores (gallium-corrole and BODIPYs) and do not show any new bands or broadening of the base peaks,
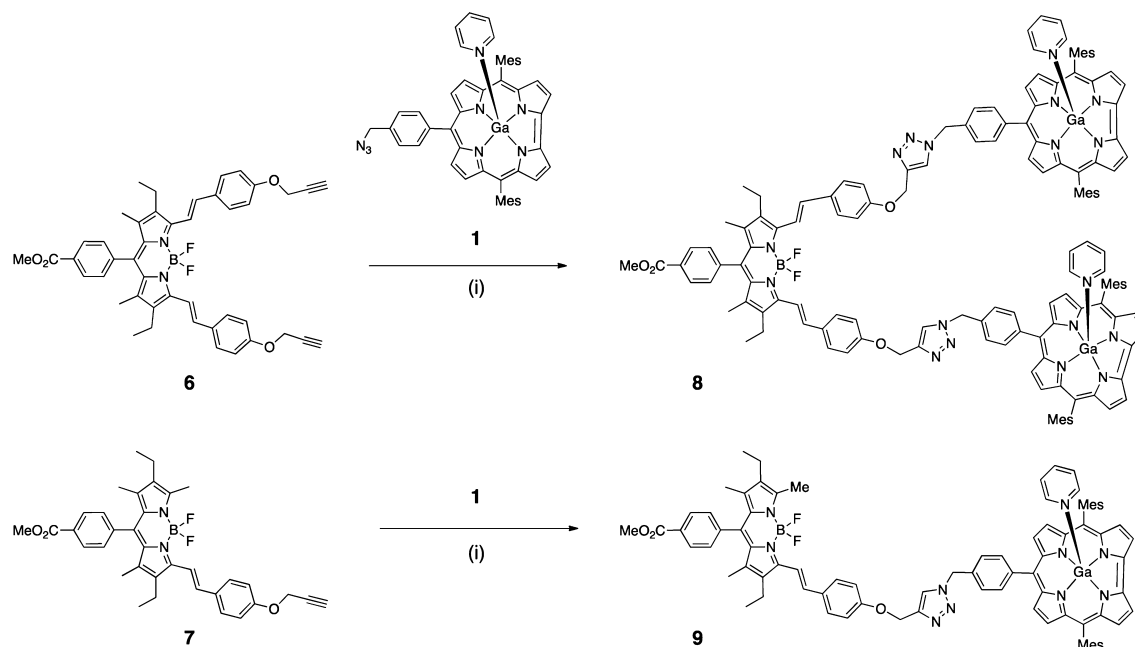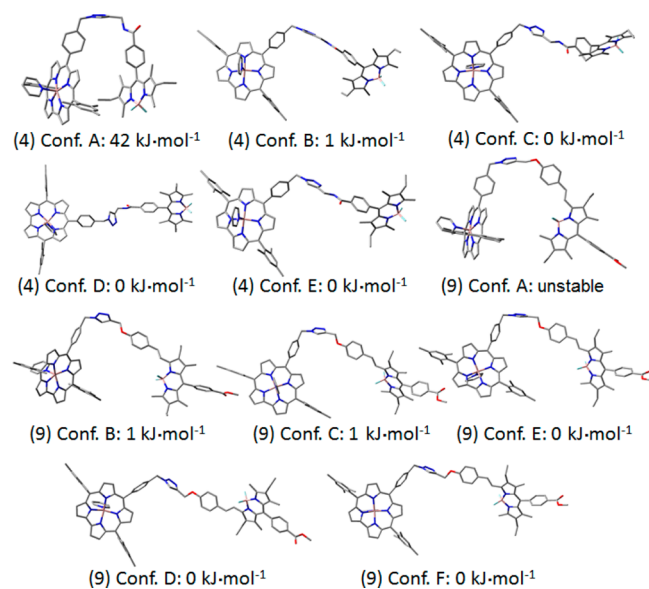
Scheme 2. Synthesis of Compounds 2, 3, 6, and 7[a]

[a](i) HOBT, EDCI·HCl, DIPEA, propargylamine, DMF, RT; (ii) p-anisaldehyde, PTSA, piperidine, dry toluene, reflux; (iii) 4-(prop-2-yn-1-yloxy)-benzaldehyde, PTSA, piperidine, dry toluene, reflux.

Scheme 3. Synthesis of Compounds 4 and 5

suggesting that electronic mixing between chromophores is minimal or nonexistent. The absorption spectra of gallium-corrole lack any significant absorption intensity in the region from 450 to 520 nm, thus allowing for selective excitation of the BODIPY donor chromophore for the examination of energy transfer (ET) processes from red BODIPY to gallium-corrole. Inversely, the absorption spectra of BODIPYs **3** and **6** lack any significant absorption intensity in the region from 460 to 550 nm, thus allowing for selective excitation of the gallium-corrole donor chromophore for the examination of ET processes from gallium-corrole to blue BODIPY.

Steady-State Fluorescence Spectroscopy and Lifetimes. Figure 2 shows the absorption, fluorescence, and excitation spectra of gallium-corrole **1** and of the (red) unfunctionalized, (green) mono-, and (blue) distyryl-BODIPY

precursors **2**, **7**, and **3**. These spectra show that the introduction of conjugated styryl substituent on BODIPY induces a bathochromic shift of the absorption and fluorescence bands. Gallium-corrole **1** exhibits a strong fluorescence band at 612 nm and a weaker vibronic shoulder at 670 nm. The fluorescence quantum yield is 0.11. The BODIPYs **2**, **3**, **6**, and **7** display an intense emission band at 543, 681, 684, and 603 nm, respectively.

Figure 3 shows the absorption, fluorescence, and excitation spectra of the bichromophoric species **4**, **5**, **8**, and **9**. Each dyad displays a fluorescence band near 612 nm readily attributable to the fluorescence of the gallium-corrole unit and a luminescence band due to the BODIPY moiety placed either at higher energy (for **4**, 540 nm) or at lower energies (for **5** and **8**, 675 and 676 nm, respectively), depending on the number of styryl groups

Scheme 4. Synthesis of Compounds 8 and 9[a]

[a](i) CuI, DIPEA, THF, N$_2$, RT.

(4) Conf. A: 42 kJ·mol^{-1} (4) Conf. B: 1 kJ·mol^{-1} (4) Conf. C: 0 kJ·mol^{-1}

(4) Conf. D: 0 kJ·mol^{-1} (4) Conf. E: 0 kJ·mol^{-1} (9) Conf. A: unstable

(9) Conf. B: 1 kJ·mol^{-1} (9) Conf. C: 1 kJ·mol^{-1} (9) Conf. E: 0 kJ·mol^{-1}

(9) Conf. D: 0 kJ·mol^{-1} (9) Conf. F: 0 kJ·mol^{-1}

Figure 1. Some optimized geometries of compounds **4** and **9** in various conformations, notably folded and unfolded, indicating the relative stabilization energies with respect to the lowest-energy conformations arbitrarily set at 0. Conformation A for compound **9** does not lead to any stable conformation upon geometry optimization. This conformation simply unfolds.

present. For compound **9**, only one band is observed at 603 nm, which is attributed to both the BODIPY and gallium-corrole units (i.e., strong fluorescence superposition). On the basis of the fluorescence positions, the BODIPY chromophore can act as an energy donor (such as in **4**) and the energy acceptor (such as in **5** and **8**). In compound **9**, this role is not well-defined when only based on these spectra.

The excitation spectra of the arrays exhibit a perfect match with the absorption, confirming the efficient energy between the two chromophores, following an excitation of the donor.

Table 1. UV−Vis Absorption Data in 2-MeTHF at 298 K

	λ_{abs} (max) (nm) ($\varepsilon \times 10^{-3}$ M^{-1} cm^{-1})				
	298 K			77 K	
	corrole		BODIPY	corrole	BODIPY
dye	Soret band	Q bands	S$_1$ band	Q bands	S$_1$ band
1	418 (206)	532 (8.69)		529	
		566 (12.7)		557, 570	
		599 (27.1)		605, 619	
2			525 (89.5)		492, 526
3			654 (92.8)		614, 674
4	419 (104)	566 (7.60)	525 (59.2)		
		599 (21.9)			
5	419 (164)	566 (16.8)	653 (66.6)		
		607 (40.7)			
6			654 (85.1)		612, 670
7			587 (81.2)		550, 597
8	419 (109)	567 (32.2)	657 (47.2)		
		606 (34.5)			
9	419 (137)		591 (81.5)		

However, the presence of two emission bands for the arrays (one for the corrole and one for the BODIPY) indicates that a part of the energy of the donor is not transferred to the acceptor, generating a residual emission attributed to the donor (cf. Figure 3).

The fluorescence data of all compounds at 298 and 77 K are summarized in Tables 2 and 3. The model BODIPY compounds **2**, **3**, **6**, and **7** exhibit high fluorescence quantum yields Φ_F ranging between 0.42 for compound **3** and 0.76 for compound **7**. The fluorescence lifetimes τ_F range from 4.64 ns for compound **2** to 7.03 ns for compound **3**. Gallium-corrole **1** displays a lower Φ_F (i.e., $\Phi_F = 0.11$, $\tau_F = 2.17$ ns) with respect to BODIPY, consistent with the literature.[23] The Φ_F values of the dyads were determined using an excitation wavelength where the donor absorbs more, bearing in mind that singlet−
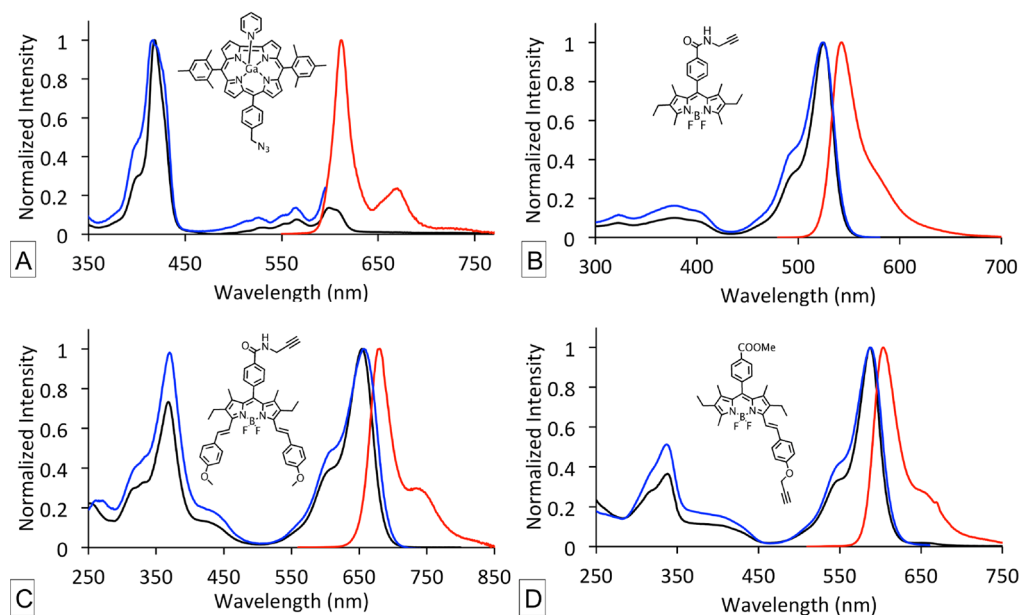
Figure 2. (black) Absorption, (red) emission, and (blue) excitation spectra of (a) gallium-corrole **1** (λ_{ex} = 540 nm, λ_{em} = 650 nm), (b) BODIPY **2** (λ_{ex} = 470 nm, λ_{em} = 590 nm), (c) BODIPY **3** (λ_{ex} = 550 nm, λ_{em} = 750 nm), and (d) BODIPY **7** (λ_{ex} = 510 nm, λ_{em} = 670 nm) in 2-MeTHF at 298 K.
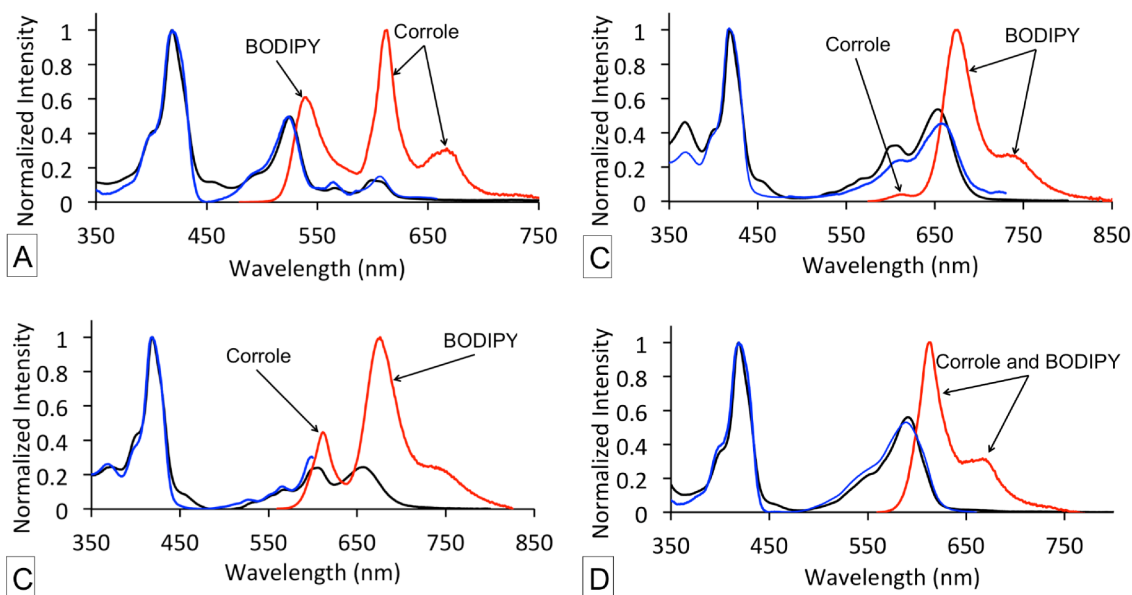

Figure 3. (black) Absorption, (red) emission, and (blue) excitation spectra of (a) dyad **4** (λ_{ex} = 470 nm, λ_{em} = 670 nm) and compounds (b) **5** (λ_{ex} = 550 nm, λ_{em} = 740 nm), (c) **8** (λ_{ex} = 550 nm, λ_{em} = 670 nm), and (d) **9** (λ_{ex} = 510 nm, λ_{em} = 670 nm) in 2-MeTHF at 298 K.

singlet energy transfer may occur and contribute to the observed intensity of the acceptor. However, these Φ_F values turn out to be lower than that of their BODIPY (**3**) and gallium-corrole (**1**) precursors (i.e., 0.016 for compound **8** and 0.093 for compound **5**), indicating that some additional nonradiative processes occur, namely, internal conversion (k_{ic}) S₁ ∼> S₀.

The fluorescence lifetimes (τ_F) of each dyad were measured separately at the fluorescence maxima of the gallium-corrole and the BODIPY chromophores at 298 and 77 K. Dyad **4** exhibits two emissions from the BODIPY (donor, 540 nm) and the gallium-corrole unit (acceptor, 613 nm; τ_F = 1.9 ± 0.1 (298 K), 2.6 ± 0.1 (77 K)). In comparison with the model compound **1** (τ_F = 2.2 ± 0.1 (298 K), 3.2 ± 0.1 (77 K)) acting

as the acceptor, the slight decrease in τ_F indicates the presence of a small nonradiative process associated with the incorporation of the flexible chain also called "loose bolt" effect (which takes part in the internal conversion rate, k_{ic}).[25] Its rate can be approximated by $k_{LB} = (1/\tau_F(\mathbf{4}\text{-``Ga''}) - (1/\tau_F(\mathbf{1})) \approx 7.2 \times 10^7$ s⁻¹, where $\tau_F(\mathbf{4}\text{-``Ga''})$ is the fluorescence lifetime of the acceptor chromophore (i.e., gallium-corrole) and $\tau_F(\mathbf{1})$ is the lifetime of the gallium-corrole model compound. This estimation is relevant with regard to the added uncertainties in the evaluation of the slower rates of energy transfers below. Concurrently, the fluorescence decay of the BODIPY residue is biphasic in dyad **4** (τ_F (in ns) = 0.7 ± 0.3 (52%) and 3.0 ± 0.1 (48%) at 298 K; 1.7 ± 0.4 (71%) and 4.5 ± 0.6 (29%) at 77 K) and is shorter than that measured for the BODIPY-containing

Table 2. Fluorescence Quantum Yields (Φ_F) and Emission Maxima

| | | λ_{em} (max) (nm) | | | |
| | | 298 K | | 77 K | |
dye	$\Phi_F{}^a$	corrole	BODIPY	corrole	BODIPY
1	0.11^c	612, 670		616, 671	
2	0.59^b		543		539, 569
3	0.42^d		681		696, 750
4	$0.036^{b,e}$	613, 667	540	616, 671	534, 565
5	$0.093^{d,e}$	613	675	608	680, 744
6	0.44^d		684		689, 744
7	0.76^c		603		611, 655
8	$0.016^{d,e}$	611	676	610	678, 742
9	$0.082^{c,e}$	613, 667		611, 668	651

^{a}The quantum yields, Φ_F, were measured in 2-MeTHF at 298 K. All Φ are corrected for changes in refractive index. ^{b}Reference = rhodamine 6G ($\Phi_F = 0.94$ in methanol). ^{c}Reference = cresyl violet ($\Phi_F = 0.54$ in methanol). ^{d}Reference = rhodamine 101 ($\Phi_F = 1.00$ in methanol).[10,11,24] ^{e}Total quantum yield (BODIPY and corrole).

model compound **2** ($\tau_F = 4.6 \pm 0.1$ (298 K) and 9.7 ± 0.3 (77 K)). The short component is clearly faster than that for compound **2** by ~6−7 fold and is consistent with the presence of an efficient energy transfer process (BODIPY*→gallium-corrole). This efficiency of ET is obtained from $ET_{eff} = ((1/\tau_F) - (1/\tau_F°))/(1/\tau_F)$ (where $\tau_F°$ and τ_F are, respectively, the fluorescence lifetimes of donor in the absence and presence of an acceptor), and the data are placed in Table 4. This value is in the order of 85 and 82% at 298 and 77 K, respectively, in this case. The presence of a second component suggests that at least two conformations, associated with the possible folding and unfolding of the flexible chain, exist in solution. The possibility that the loose bolt effect contributes to the decrease in τ_F exists, but the calculated rate $(1/\tau_F(4\text{-“BODIPY”})) - (1/\tau_F(\mathbf{2}))$, where $\tau_F(4\text{-“BODIPY”})$ is the lifetime of the slow component of the BODIPY fluorescence decay, gives a value (~1.2×10^8 s^{-1}) that is only ~2-fold larger than the k_{LB} evaluated for the gallium-corrole chromophore in compound **4** (i.e., ~7.2×10^7 s^{-1}). Similarly, dyad **5** exhibits a blue BODIPY acting as the energy acceptor with τ_F (in ns) = 3.6 ± 0.1 (298 K) and $5.8 \pm$

Table 4. Energy Transfer Rates (k_{ET}) Calculated with eq 1 (2-MeTHF)

| | | k_{ET} (10^8 s^{-1}) | |
	D*→A	298 K	77 K
4	(red-BODIPY* → Cor)^a	12 (85%)	4.9 (82%)
		$1.2\ (35\%)^b$	$1.2\ (54\%)^b$
5	(Cor* → blue-BODIPY)	45 (91%)	17 (84%)
		$0.7\ (13\%)^b$	no transfer
8	(Cor* → blue-BODIPY)	$1.7\ (27\%)^b$	$0.4\ (13\%)^b$
9	(green-BODIPY*→Cor)	$0.8\ (30\%)^b$	$1.0\ (40\%)^b$
	(Cor*→green-BODIPY)	$1.0\ (18\%)^b$	$0.4\ (12\%)^b$

^{a}Cor = gallium-corrole chromophore. ^{b}This value is most likely mixed with the loose bolt effect, and thus no reliable value for k_{ET} can be extracted.

0.1 (77 K). These values are also shorter than that for the model compound **3** (τ_F (in ns) = 6.3 ± 0.1 and 12.1 ± 0.3). The estimated k_{LB} values are 1.2×10^8 (298 K) and 0.9×10^8 s^{-1} (77 K). This qualitative analysis indicates that the contribution of k_{LB} in the dyads ranges from ~0.7×10^8 to ~1.2×10^8 s^{-1}, and the conclusion is that the apparent deactivation rates evaluated for slow processes are most likely composed of two contributions, namely, k_{ET} (rate of energy transfer) and k_{LB}, which may be of comparable sizes. Table 3 summarizes all the τ_F data and can be separated into two categories: the flexible chain is placed near (**2−5**) or far (**6−9**) from the BF$_2$ unit. The main reason for this separation is that the fluorescence decays of the donor exhibit a double exponential for compounds **4** and **5** (presumably due to a chain folding) but not in dyads **8** and **9**. The flexible chains in these two series slightly differ by the presence of a (C=O)NH in the former sets instead of an −O− link used in the second series.

Singlet Energy Transfer Rates. The rate of energy transfer (i.e., k_{ET}) for each dyad was evaluated using the τ_F data placed in Table 3. The k_{ET} values were calculated using eq 1:

$$k_{ET} = \left(\frac{1}{\tau_F} - \frac{1}{\tau_F°} \right) \tag{1}$$

Table 3. Fluorescence Lifetimes (τ_F) in 2-MeTHF

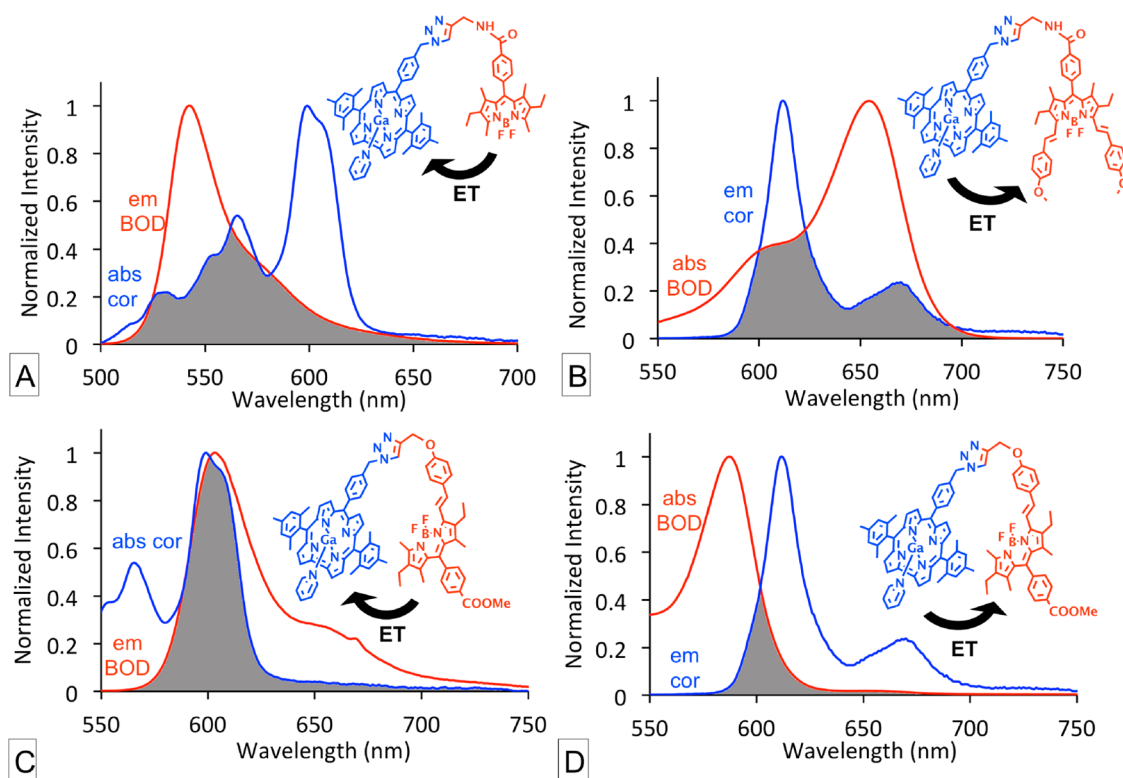| | | 298 K | | | 77 K | | |
dye	λ_{exc} (nm)	λ_{em} (nm)	τ_{F1} (ns) (rel. int.)	τ_{F2} (ns) (rel. int.)	λ_{em} (nm)	τ_{F1} (ns) (rel. int.)	τ_{F2} (ns) (rel. int.)
1	527	612	2.2 ± 0.1		619	3.2 ± 0.1	
2	470	543	4.6 ± 0.1		540	9.7 ± 0.3	
3	550	681	6.3 ± 0.1		695	12.1 ± 0.3	
4	470	540	0.7 ± 0.3 (0.52)	3.0 ± 0.1 (0.48)	534	1.7 ± 0.4 (0.71)	4.5 ± 0.6 (0.29)
		613	1.9 ± 0.1		615	2.6 ± 0.1	
5	550	611	0.2 ± 0.1 (0.87)	1.9 ± 0.1 (0.13)	611	0.5 ± 0.2 (0.68)	3.3 ± 0.1 (0.32)
		675	3.6 ± 0.1		679	5.8 ± 0.1	
6	510	684	7.0 ± 0.1		690	11.9 ± 0.4	
7	510	603	5.4 ± 0.1		611	6.8 ± 0.1	
8	550	611	1.6 ± 0.1		610	2.8 ± 0.1	
		676	3.7 ± 0.2		678	5.0 ± 0.1	
9	510	613	1.8 ± 0.1		611	2.6 ± 0.1	
		667	3.8 ± 0.2		666	4.1 ± 0.1	

Figure 4. Superposition of the normalized absorption and fluorescence spectra in 2-MeTHF at 298K of (A) **1** (blue) (ε: 27 100 M^{-1} cm^{-1}) with **2** (red), (B) **3** (red) (ε: 92 800 M^{-1} cm^{-1}) with **1** (blue), (C) **1** (blue) (ε: 27 100 M^{-1} cm^{-1}) with **7** (red), and (D) **7** (red) (ε: 81 200 M^{-1} cm^{-1}) with **1** (blue). The absorption and fluorescence spectra of the BODIPYs and gallium-corroles are in red and blue, respectively. The overlaps are shaded in gray. Note that the folded conformation drawn for the dyads is only to make them fit within the graphs.

Table 5. Values of J, $k_F°(D)$, k_{ET}(cal), and k_{ET}(exp) for dyads 4, 5, and 9 (Both Directions) at 298 K

	ET direction	θ_A (deg)	θ_D (deg)	ϕ (deg)	κ^{2a}	r^a (Å)	k_{ET}(cal) (10^8 s^{-1})	k_{ET}(exp) (10^8 s^{-1})	k_{ET}(cal)/k_{ET}(exp)
	$k_F° = 1.28 \times 10^8$ s^{-1b}								
	$J = 2.7 \times 10^{-14c}$								
4B	red BODIPY*→Cor	129.6	134.3	19.6	0.2	17.9	47	12	3.9
4C	red-BODIPY*→Cor	55.7	120.5	67.7	1.5	18.7	272	12	23
4D	red-BODIPY*→Cor	88.0	97.3	58.1	0.3	21.1	26	12	2.2
4E	red-BODIPY*→Cor	57.4	119.0	56.8	1.8	19.0	298	12	25
	$k_F° = 0.50 \times 10^8$ s^{-1}								
	$J = 34 \times 10^{-14}$								
5B	Cor*→blue-BODIPY	129.6	134.3	19.6	0.2	17.9	231	45	5.1
5C	Cor*→blue-BODIPY	55.7	120.5	67.7	1.5	18.7	1338	45	30
5D	Cor*→blue-BODIPY	88.0	97.3	58.1	0.3	21.1	128	45	2.8
5E	Cor*→blue-BODIPY	57.4	119.0	56.8	1.8	19.0	1465	45	32
	$k_F° = 0.67 \times 10^8$ s^{-1}								
	$J = 5.2 \times 10^{-14}$								
9B	green-BODIPY*→Cor	82.7	95.0	81.5	0.03	16.5	12	0.8^d	15^d
9C	green-BODIPY*→Cor	98.9	148.0	50.3	0.1	17.5	27	0.8^d	34^d
9D	green-BODIPY*→Cor	56.9	113.4	26.2	2.4	22.3	153	0.8^d	190^d
9E	green-BODIPY*→Cor	94.2	149.9	32.6	0.4	17.1	125	0.8^d	156^d
9F	green-BODIPY*→Cor	100.0	129.6	27.0	0.3	20.7	30	0.8^d	37^d
	$k_F° = 0.50 \times 10^8$ s^{-1}								
	$J = 4.1 \times 10^{-14}$								
9B	Cor*→green-BODIPY	82.7	95.0	81.5	0.03	16.5	7	1.0^d	7^d
9C	Cor*→green-BODIPY	98.9	148.0	50.3	0.1	17.5	16	1.0^d	16^d
9D	Cor*→green-BODIPY	56.9	113.4	26.2	2.4	22.3	90	1.0^d	90^d
9E	Cor*→green-BODIPY	94.2	149.9	32.6	0.4	17.1	74	1.0^d	74^d
9F	Cor*→green-BODIPY	100.0	129.6	27.0	0.3	20.7	18	1.0^d	18^d

^{a}The r and κ^2 values result from the DFT computations (optimized geometries; Figure 1). ^{b}$k_F°(D) = \Phi_F(D)/\tau_F(D)$; these data are from Tables 2 and 3, respectively. ^{c}Cor = gallium-corrole chromophore. **J** is in mmol^{-1} cm^6. ^{d}This value is unreliable due to the loose bolt effect (see text).

3400

dx.doi.org/10.1021/ic402798f | *Inorg. Chem.* 2014, 53, 3392−3403

where $\tau_F{}^\circ$ and τ_F are, respectively, the fluorescence lifetimes of donor in the absence and presence of an acceptor. Thus, these values are extracted from the model compounds (**2**, **3**, **6**, and **7**) and dyads (**4**, **5**, **8**, and **9**), respectively. This method is more accurate than measuring the Φ_F values for strongly overlapping fluorescence and absorption spectra, as both the area under the corrected fluorescence spectrum and the exact absorbance of the donor chromophore are not accessible with enough precision. The k_{ET} values are summarized in Table 4; the values marked with footnote-b indicate that the value is most likely mixed with the loose bolt effect k_{LB}, and consequently the only reliable conclusion is that the energy transfer process is either nonexistent or too slow to reliably access k_{ET}.

Singlet Energy Transfer Analysis. The Förster theory[26] is used to interpret the experimental k_{ET} values of the dyads **4**, **5**, **8**, and **9**. The calculated rates of energy transfer are obtained using eq 2:

$$k_{ET} = \frac{8.8 \times 10^{-25} \kappa^2 k_F{}^\circ(D)}{n^4 r^6} \times J \tag{2}$$

where $k_F{}^\circ(D) = \Phi_F{}^\circ/\tau_F{}^\circ$, with $\Phi_F{}^\circ$ being the fluorescence quantum yield of the donor in the absence of the acceptor, r is the center-to-center donor−acceptor separation, n is the refractive index of the solvent (here 1.406), κ^2 is an orientation factor describing the relative orientation of the electronic dipole moments of the associated transitions of the donor and acceptor ($\kappa^2 = (\sin(\theta_D)\sin(\theta_A)\cos(\phi) - 2\cos(\theta_D)\cos(\theta_A))^2$, where θ_D and θ_A are the angles made by the donor−acceptor vector with the transition moment vector of the donor and acceptor, respectively). For both BODIPY and gallium-corrole units, the transition moment is oriented along the center of the chromophore toward C_{meso}. J is the spectral overlap ($\int F_D(\lambda) \varepsilon_A(\lambda)\lambda^4 d\lambda / \int F_D(\lambda)d\lambda$, in mmol^{-1} cm^6, also called the J integral) of the donor fluorescence spectra ($F_D(\lambda)$) and the acceptor absorption profile ($\varepsilon_A(\lambda)$). Figure 4 overlays the fluorescence spectra of the donors with the absorption spectra of the acceptors of the necessary model compounds building the dyads. For **9**, the proximity of the absorption and fluorescence bands for both units makes J non-nil for both directions and should be considered.

The calculated (cal) values of J, $k_F{}^\circ(D)$, structural parameters (r, ϕ, θ_D, θ_A), k_{ET}(cal), and k_{ET}(exp) for dyads **4**, **5**, and **9** (both directions) are placed in Table 5. In the absence of X-ray structures, structural parameters were extracted from DFT calculations (B3LYP; geometry optimizations placed in Figure 1). The J values compare favorably to that recently reported for a pyrene−BODIPY dyad (Figure 5).[27] The calculated k_{ET} values are ~2 to ~30 times larger than the experimental ones for compounds **4** and **5**. For compound **9**, this ratio is larger but unreliable. This situation is not uncommon as it has been
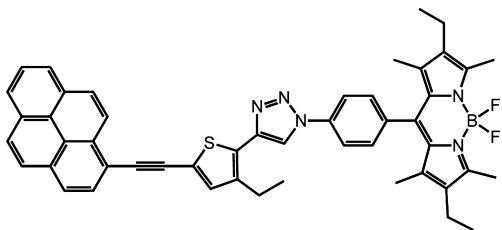
encountered before where a ratio of k_{ET}(cal)/k_{ET}(exp) between 11 to 31 was noted.[28] The main reason for this is that the Förster approach is considered an approximation.[29] Nonetheless, comparisons are still possible.

One important issue is that the relative size of both k_{ET}(exp) and k_{ET}(cal) between compounds **4** and **5** (same flexible chain) and **9** (two directions, so same flexible chain) follow the same relative trend. Indeed, the values of both k_{ET}(cal) and k_{ET}(exp) are ~5 times larger for compound **5** than are those for **4**. This comparison indicates that the dominant parameter for this effect is the J integral, which is ~10 times larger for compound **5** by virtue of the larger absorptivity of the acceptor (for compound **3**, ε = 92 800 M^{-1} cm^{-1}). For compound **9**, the values of both k_{ET}(cal) and k_{ET}(exp) are larger for the green-BODIPY*→Cor process than they are for the Cor*→green-BODIPY process. In this case, both $k_F{}^\circ(D)$ and J contribute to the larger size of k_{ET}. It is also interesting to note that the k_{ET}(cal) values for **4** and **5** falls into two groups, slow and fast rates, where ~1 order of magnitude separates the two groups. This observation corroborates well with the presence of two τ_F values (i.e., two k_{ET} values) in these cases, suggesting that two families of conformations provide similar rates, namely, directed by κ^2.

However, one issue needs to be addressed. The k_{ET} values for the recently reported pyrene−BODIPY dyad (Figure 5) are faster by 1 to 2 orders of magnitude than those reported here.[27] The authors assumed (based on the Förster theory) that the center-to-center distance is 20 Å (similar to the unfolded conformations investigated here), which is the distance between the center of pyrene and the center of BODIPY. However, the pyrene unit is conjugated all the way to the triazole linker (i.e., N-phenyl position), and so the effective distance is much shorter than 20 Å. Indeed, by changing 20 by 9.6 Å in eq 2, the calculated k_{ET} increases by 2 orders of magnitude. Moreover, a relationship between the C_{meso}−C_{meso} distance (not center-to-center) and k_{ET} was demonstrated for a series of cofacial bisporphyrins,[30] and also demonstrated was that any atom or group placed exactly between the closest positions (i.e., closest carbons) between the donor and the acceptor slowed down the energy transfer process.[31] The selection of the correct r value turns out to be a difficult task. In addition, the Dexter mechanism can also contribute to the overall process for this pyrene−BODIPY (Figure 5). Consequently, k_{ET}(total) can be the sum of both contributions, that is, the Förster and the Dexter, and this despite unfavorable dihedral angles between the phenyl group and the donor and acceptor moieties. This phenomenon, where unfavorable dihedral angles are present and yet efficient energy transfers occur, was recently demonstrated by us for truxene-containing polyporphyrin dyads.[32] The obvious absence of conjugation in the compounds investigated in this work and the large donor−acceptor separations (avoiding any orbital overlap) preclude this mechanism. Considering these parameters, the k_{ET} values for dyads **4**, **5**, **8**, and **9** are bound to be significantly slower than that reported for the pyrene−BODIPY dyad of Figure 5.

■ CONCLUSION

Dyads incorporating various types of BODIPY chromophores, here called red, green, and blue, and gallium-corroles have been synthesized in good yields using the click chemistry. The direction of the singlet energy transfer, gallium-corrole*→ BODIPY or BODIPY*→ gallium-corrole, can be modulated depending on whether zero, one, or two styryl groups are

Figure 5. Structure of the recently investigated dyad pyrene−BODIPY.

attached to the BODIPY moiety. In one case, both directions were found possible based upon the non-nil spectral overlap of the donor emission and acceptor absorption (i.e., J integral of the Förster theory). The qualitative analysis of the k_{ET} data using FRET clearly corroborates the presence of conformers in solution; the folded conformers are more stable for compounds **4** and **5**, and the unfolded one is more stable for compound **9**, which uses slightly different flexible chains. The size of the J integral plays a key role on the size of the k_{ET} value.

■ ASSOCIATED CONTENT

Ⓢ Supporting Information

Comparison of absorbance and emission spectra of compounds **2**, **7**, and **3**. ^{1}H NMR spectra, mass spectra, and superposition of absorption and excitation spectra of each compound. This material is available free of charge via the Internet at http://pubs.acs.org.

■ AUTHOR INFORMATION

Corresponding Authors

*E-mail: claude.gros@u-bourgogne.fr. Phone: 33 (0)3 80 39 61 12. Fax: 33 (0)3 80 39 61 17. (C.P.G.)
*E-mail: christine.goze@u-bourgogne.fr. Phone: 33 (0)3 80 39 90 43. Fax: 33 (0)3 80 39 61 17. (C.G.)
*E-mail: pierre.harvey@USherbrooke.ca. Phone: 819-821-7092. Fax: 819-821-8017. (P.D.H.)

Notes

The authors declare no competing financial interest.

■ ACKNOWLEDGMENTS

■ REFERENCES

(1) (a) Bandi, V.; Ohkubo, K.; Fukuzumi, S.; D'Souza, F. *Chem. Commun.* **2013**, *49* (28), 2867−2869. (b) Lee, C. Y.; Hupp, J. T. *Langmuir* **2010**, *26* (5), 3760−3765. (c) Leonardi, M. J.; Topka, M. R.; Dinolfo, P. H. *Inorg. Chem.* **2012**, *51* (24), 13114−13122.

(2) Shao, W.; Wang, H.; He, S.; Shi, L.; Peng, K.; Lin, Y.; Zhang, L.; Ji, L.; Liu, H. *J. Phys. Chem. B* **2012**, *116* (49), 14228−14234.

(3) (a) Barbe, J. M.; Canard, G.; Brandès, S.; Guilard, R. *Eur. J. Org. Chem.* **2005**, *21*, 4601−4611. (b) El Ojaimi, M.; Gros, C. P.; Barbe, J.-M. *Eur. J. Org. Chem.* **2008**, *7*, 1181−1186. (c) Gros, C. P.; Barbe, J.-M.; Espinosa, E.; Guilard, R. *Angew. Chem. Int. Ed. (VIP Communication)* **2006**, *45*, 5642−5645. (d) Guilard, R.; Gros, C. P.; Barbe, J.-M.; Espinosa, E.; Jérôme, F.; Tabard, A.; Shao, J.; Ou, Z. P.; Latour, J.-M.; Kadish, K. M. *Inorg. Chem.* **2004**, *43*, 7441−7455. (e) Guilard, R.; Gros, C. P.; Bolze, F.; Jérôme, F.; Ou, Z. P.; Shao, J. G.; Fischer, J.; Weiss, R.; Kadish, K. M. *Inorg. Chem.* **2001**, *40* (19), 4845−4855. (f) Guilard, R.; Jérôme, F.; Barbe, J. M.; Gros, C. P.; Ou, Z. P.; Shao, J.; Fischer, J.; Weiss, R.; Kadish, K. M. *Inorg. Chem.* **2001**, *40* (19), 4856−4865. (g) Jérôme, F.; Gros, C. P.; Tardieux, C.; Barbe, J.-M.; Guilard, R. *Chem. Commun.* **1998**, 2007−2008. (h) Kadish, K. M.; Ou, Z. P.; Shao, J.; Gros, C. P.; Barbe, J.-M.; Jérôme, F.; Bolze, F.; Burdet, F.; Guilard, R. *Inorg. Chem.* **2002**, *41*, 3990−4005. (i) Kadish, K. M.; Shao, J.; Ou, Z. P.; Gros, C. P.; Bolze, F.; Barbe, J.-M.; Guilard, R. *Inorg. Chem.* **2003**, *42*, 4062−4070.

(4) (a) Agadjanian, H.; Ma, J.; Rentsendorj, A.; Valluripalli, V.; Hwang, J. Y.; Mahammed, A.; Farkas, D. L.; Gray, H. B.; Gross, Z.; Medina-Kauwe, L. K. *Proc. Natl. Acad. Sci. U.S.A.* **2009**, *106* (15), 6105−6110. (b) Hwang, J. Y.; Lubow, D. J.; Sims, J. D.; Gray, H. B.; Mahammed, A.; Gross, Z.; Medina-Kauwe, L. K.; Farkas, D. L. *J. Biomed. Opt.* **2012**, *17* (1), 015003. (c) Lim, P.; Mahammed, A.; Okun, Z.; Saltsman, I.; Gross, Z.; Gray, H. B.; Termini, J. *Chem. Res. Toxicol.* **2012**, *25* (2), 400−409. (d) Shi, L.; Jiang, H.-F.; Yin, W.; Wang, H.-H.; Wang, H.; Zhang, L.; Ji, L.-N.; Liu, H.-Y. *Wuli Huaxue Xuebao* **2012**, *28* (2), 465−469.

(5) (a) Liu, X.; Tripathy, U.; Bhosale, S. V.; Langford, S. J.; Steer, R. P. *J. Phys. Chem. A* **2008**, *112* (38), 8986−8998. (b) Weaver, J. J.; Sorasaenee, K.; Sheikh, M.; Goldschmidt, R.; Tkachenko, E.; Gross, Z.; Gray, H. B. *J. Porphyrins Phthalocyanines* **2004**, *8* (1−3), 76−81.

(6) Aviv, I.; Gross, Z. *Chem. Commun.* **2007**, *20*, 1987−1999.

(7) (a) Bendix, J.; Dmochowski, I. J.; Gray, H. B.; Mahammed, A.; Simkhovich, L.; Gross, Z. *Angew. Chem., Int. Ed. Engl.* **2000**, *39* (22), 4048−4051. (b) Simkhovich, L.; Goldberg, I.; Gross, Z. *J Inorg. Biochem.* **2000**, *80* (3−4), 235−238.

(8) Brizet, B.; Eggenspiller, A.; Gros, C. P.; Barbe, J. M.; Goze, C.; Denat, F.; Harvey, P. D. *J. Org. Chem.* **2012**, *77* (7), 3646−3650.

(9) Eggenspiller, A.; Takai, A.; El-Khouly, M. E.; Ohkubo, K.; Gros, C. P.; Bernhard, C.; Goze, C.; Denat, F.; Barbe, J. M.; Fukuzumi, S. *J. Phys. Chem. A* **2012**, *116* (15), 3889−3898.

(10) Baumler, W.; Penzkofer, A. *Chem. Phys.* **1990**, *140*, 75−97.

(11) Magde, D.; Brannon, J. H.; Cremers, T. L.; Olmsted, J., III *J. Phys. Chem.* **1979**, *83* (6), 696−699.

(12) Brouwer, A. M. *Pure Appl. Chem.* **2011**, *83* (12), 2213−2228.

(13) Schäfer, F. P., *Topics in Applied Physics: Structure and Properties of Laser Dyes.* Springer-Verlag: Berlin, 1990; Vol. 1.

(14) Lide, D. R., *Handbook of Chemistry and Physics.* Chemical Rubber Publishing Co: Berlin, 1957.

(15) Frisch, M. J. et al. Gaussian, Inc., Wallingford CT, 2004.

(16) (a) Bauernschmitt, R.; Ahlrichs, R. *Chem. Phys. Lett.* **1996**, *256*, 454−464. (b) Becke, A. D. *J. Chem. Phys.* **1993**, *98*, 5648−5652. (c) Casida, M. E.; Jamorski, C.; Casida, K. C.; Salahub, D. R. *J. Chem. Phys.* **1998**, *108*, 4439−4449. (d) Hohenberg, P.; Kohn, W. *Phys. Rev.* **1964**, *136*, B864−871. (e) Hohenberg, P.; Kohn, W. *J. Phys. Rev.* **1965**, *140*, A1133−1138. (f) Lee, C.; Yang, W.; Parr, R. G. *Phys. Rev. B* **1988**, *37*, 785−789. (g) Miehlich, B.; Savin, A.; Stoll, H.; Preuss, H. *Chem. Phys. Lett.* **1989**, *157*, 200−206. (h) Parr, R. G.; Yang, W., *Density-functional theory of atoms and molecules.* Oxford Univ. Press: Oxford, 1989; (i) Salahub, D. R.; Zerner, M. C., *The Challenge of d and f Electrons.* Amer. Chem. Soc.: Washington, D.C., 1989; (j) Stratmann, R. E.; Scuseria, G. E.; Frisch, M. J. *J. Chem. Phys.* **1998**, *109*, 8218−8224.

(17) (a) Binkley, J. S.; Pople, J. A.; Hehre, W. J. *J. Am. Chem. Soc.* **1980**, *102*, 939−947. (b) Dobbs, K. D.; Hehre, W. J. *J. Comput. Chem.* **1986**, *7*, 359−378. (c) Dobbs, K. D.; Hehre, W. J. *J. Comput. Chem.* **1987**, *8*, 861−879. (d) Dobbs, K. D.; Hehre, W. J. *J. Comput. Chem.* **1987**, *8*, 880−893. (e) Gordon, M. S.; Binkley, J. S.; Pople, J. A.; Pietro, W. J.; Hehre, W. J. *J. Am. Chem. Soc.* **1982**, *104*, 2797−2803. (f) Pietro, W. J.; Francl, M. M.; Hehre, W. J.; Defrees, D. J.; Pople, J. A.; Binkley, J. S. *J. Am. Chem. Soc.* **1982**, *104*, 5039−5048.

(18) (a) Kondo, M.; Furukawa, S.; Hirai, K.; Kitagawa, S. *Angew. Chem., Int. Ed. Engl.* **2010**, *49*, 5327−5330. (b) Kolemen, S.; Bozdemir, O. A.; Cakmak, Y.; Barin, G.; Erten-Ela, S.; Marszalek, M.; Yum, J.-H.; Zakeeruddin, S. M.; Nazeeruddin, M. K.; Graetzel, M.; Akkaya, E. U. *Chem. Sci.* **2011**, *2*, 949−954.

(19) Saltsman, I.; Mahammed, A.; Goldberg, I.; Tkachenko, E.; Botoshansky, M.; Gross, Z. *J. Am. Chem. Soc.* **2002**, *124* (25), 7411−20.

(20) (a) Fan, J.; Hu, M.; Zhan, P.; Peng, X. *Chem. Soc. Rev.* **2013**, *42*, 29−43. (b) Dost, Z.; Atilgan, S.; Akkaya, E. U. *Tetrahedron* **2006**, *62*, 8484−8488. (c) Zhang, X. L.; Xiao, Y.; Qian, X. H. *Org. Lett.* **2008**, *10*, 29−32.

(21) (a) Garcia, G.; Naud-Martin, D.; Carrez, D.; Croisy, A.; Maillard, P. *Tetrahedron* **2011**, *67* (26), 4924−4932. (b) Kolb, H. C.; Finn, M. G.; Sharpless, K. B. *Angew. Chem., Int. Ed.* **2001**, *40* (11), 2004−2021. (c) Lahann, J., *Click Chemistry for Biotechnology and Materials Science*. Wiley: Chichester, West Sussex, 2009; (d) Locos, O. B.; Heindl, C. C.; Corral, A.; Senge, M. O.; Scanlan, E. M. *Eur. J. Org. Chem.* **2010**, *6*, 1026−1028.

(22) Takai, A.; Chkounda, M.; Eggenspiller, A.; Gros, C. P.; Lachkar, M.; Barbe, J.-M.; Fukuzumi, S. *J. Am. Chem. Soc.* **2010**, *132*, 4477−4489.

(23) Weaver, J. J. PhD Thesis. Califonia Institute of Technology, Pasadena (USA), 2005.

(24) Drexhage, K. H. *J. Res. Natl. Bur. Stand. A, Phys. Chem.* **1976**, *80*, 421−428.

(25) Berezin, M. Y.; Achilefu, S. *Chem. Rev.* **2010**, *110*, 2641−2684.

(26) Förster, T. *Ann. Phys.* **1948**, *2*, 55−75.

(27) Bai, D.; Benniston, A. C.; Hagon, J.; Lemmetyinen, H.; Tkachenko, N. V.; Harrington, R. W. *Phys. Chem. Chem. Phys.* **2013**, *15*, 9854−9861.

(28) Cho, H. S.; Jeong, D. H.; Yoon, M.-C.; Kim, Y.-H.; Kim, Y.-R.; Kim, D.; Jeong, S. C.; Kim, S. K.; Aratani, N.; Shinmori, H.; Osuka, A. *J. Phys. Chem. A* **2001**, *105*, 4200−4210.

(29) (a) Beljonne, D.; Curutchet, C.; Scholes, G. D.; Silbey, R. J. *J. Phys. Chem. B* **2009**, No. 113, 6583−6599. (b) Curutchet, C.; Mennucci, B.; Scholes, G. D.; Beljonne, D. *J. Phys. Chem. B* **2008**, *112*, 3759−3760. (c) Khan, Y. R.; Dykstra, T. E.; Scholes, G. D. *Chem. Phys. Let.* **2008**, *461*, 305−309. (d) Scholes, G. D. *Annu. Rev. Phys. Chem.* **2003**, *54*, 57−87.

(30) Faure, S.; Stern, C.; Guilard, R.; Harvey, P. D. *J. Am. Chem. Soc.* **2004**, *126*, 1253−1261.

(31) (a) Gros, C. P.; Aly, S. M.; El Ojaimi, M.; Barbe, J.-M.; Brisach, F.; Abd-El-Aziz, A. S.; Harvey, P. D. *J. Porphyrins Phthalocyanines* **2007**, *11* (3−4), 244−257. (b) Gros, C. P.; Brisach, F.; Meristoudi, A.; Espinosa, E.; Guilard, R.; Harvey, P. D. *Inorg. Chem.* **2007**, *46*, 125−135.

(32) Langlois, A.; Xu, H.-X.; Brizet, B.; Denat, F.; Barbe, J.-M.; Gros, C. P.; Harvey, P. D. *J. Porphyrins Phthalocyanines* **2014**, *19*, 94−106.